 https://doi.org/10.3311/PPci.19740

Periodica Polytechnica Civil Engineering, 66(4), pp. 1060–1070, 2022

Prediction of In-plane Stiffness for the Cold-formed Steel Frame of the Wall Panel Structure

Apai Benchaphong[1], Rattanasak Hongthong[1], Chitsirin Konkong[2], Nirut Konkong[3*]

[1] Faculty of Engineering, Rajamangala University of Technology Krungthep, Bangkok 10120, Thailand
[2] Faculty of Science and Technology, Pibulsongkram Rajabhat University, Phitsanulok 65000, Thailand
[3] Irrigation Office 3 - Royal Irrigation Department, Phitsanulok 65000, Thailand
[*] Corresponding author, e-mail: nirut.k@ku.th

Received: 22 December 2021, Accepted: 17 June 2022, Published online: 07 July 2022

Abstract

The purpose of this research was to study the lateral deformation behavior of cold-formed steel wall panel structures using experimental tests, finite element analysis and analytical methods to study the lateral stiffness of these structures. The wall panel structures were tested by full-scale experiments the experimental results of which were verified by a 3D-finite element model. The verification results showed a good correlation between the experimental tests and a finite element model. The single-column spring model was proposed for an elastic lateral stiffness analysis of the cold-formed steel wall panel structures that were formed by combinations of a guide cantilever beam and springs connection. The spring constants were defined by using the stiffness of the stub-chord connection and the bending stiffness of the chord. The experiments tests and finite element analysis were used to verify this single-column spring model. The comparison results showed good agreement between the analytical prediction, finite element analysis and experimental data in the case of the primary type of cold-formed wall structure. The proposed procedure was an efficient method for elastic lateral deformation analysis of cold-formed wall panel structures which can be used for such configurations.

Keywords

wall structure, cold-formed steel, lateral stiffness, single-column spring model

1 Introduction

Cold-formed steel (CFS) has been used in many parts of building structures because it can be variously shaped and can be used in a variety of applications and can be employed in structural and non-structural building systems. For example, channel sections are often used in the construction of steel framing systems such as columns, beams, and truss structures [1–3]. Due to some unique advantages such as high strength-to-weight ratio and construction speed, cold-formed steel components have seen substantial expansion in use in the building sector in recent years.

The CFS wall panel structure (CFS-wall) is an interesting replacement for traditional wooden frames which were widely used in developed countries such as Europe and the United States [4–6]. CFS-wall is an important element that resists the lateral force normally applied to buildings. In construction applications, CFS- walls consist of cold-formed steel framing members and sheathing with the framing members, such as the top and bottom chord, being screwed to the stud members. The sheathing material, such as wood, steel sheet, plywood, or gypsum wallboard, was used in lateral load resisting systems and was sheathed on one or both sides with steel [7, 8]. In practical design, the engineer often neglects to predict the load capacities of CFS shear walls sheathing which has strength retardant properties. The influence of the sheathing materials and fastener spacing on this lateral behavior was studied by Liu et al. [9] whose results showed that the shear wall strength increased by approximately 10% and also modestly decreased energy dissipation. Also, the CFS-wall type asserts an influence on the load capacity of the wall [10, 11] such as the wall height to width ratio [12] and screw spacing [13]. The combined X-strap bracing with K-braced systems was analyzed by Mehran Zeynalian et al. [14] with the results showing that both the shear strength and ductility of the wall were usable in seismic regions.

The lateral stiffness of the CFS-wall was an essential parameter in the design process to address concerns of shear force distributions and lateral drift calculations

Cite this article as: Benchaphong, A., Hongthong, R., Konkong, C., Konkong, N. "Prediction of In-plane Stiffness for the Cold-formed Steel Frame of the Wall Panel Structure", Periodica Polytechnica Civil Engineering, 66(4), pp. 1060–1070, 2022. https://doi.org/10.3311/PPci.19740

under wind and earthquake loadings. Due to the complexity of the structural mechanism of the CFS-wall under the lateral force, a design recommendation procedure was proposed by [15, 16]. However, the lateral stiffness of the CFS-wall in these design recommendations was neglected. Thus, theoretical methodologies to determine lateral stiffness should be proposed.

This paper describes an experimental study in which finite element analysis and analytical methods were adopted to predict the lateral stiffness of the CFS-wall. The development of the analytical method was focused on the primary elements in the wall such as top-bottom chord members, stud members and connections.

2 Experimental tests

The experimental tests were divided into 2 sections: connection resistance tests and lateral wall resistance tests. The test specimens were prepared from CFS with a cross-section of C-74 (75.00 × 40.00 × 0.55 mm of web depth, flange size and thickness), with the nominal yield stress (f_y) of 574.22 MPa and nominal ultimate stress (f_u) of 622.31 MPa and assembled with 5.00 mm screw fasteners.

The mechanical properties of CFS procedures followed ASTM A370-07 [17] which are presented in Table 1. Self-drilling screws with a diameter of 5.00 mm and a length of 12.70 mm were used. Self-tapping screws with a diameter of 4.00 mm and a length of 25.00 mm were used to fasten the stud member to the chord member. The mechanical properties of the screws test procedures followed ASTM C1513-18 [18], as presented in Table 2.

2.1 CFS-wall connection test

The dimensions of the test specimen with a width of 1000 mm and a height of 250 mm, as shown in Fig. 1. At point A, the connection was defined as a semi-rigid connection in which a 3-screw plate was used as a fastener. At points B, C and D, the connections are defined as a pin connection using a single screw as a fastener. The details of the test settings are shown in Fig. 2. The bottom chord of the specimen was attached to the support, and the top chord was connected to a load cell by the beam transfer. 2-Linear Variable Differential Transformers (LVDTs) were installed in the top chord connection for measuring the lateral movement. The load was gradually applied until the specimen failed. Once the applied load began to drop, the specimen continued to lose lateral stability. The test was repeated 5 times.

2.2 CFS-wall lateral test

Experimental tests were performed on the wall panel specimens with dimensions of 1,000 mm in width and 2,000 mm in height with a rectangular geometry as shown in Table 3.

The top-bottom chords and stud members of the walls were constructed of channel sections with C-74. At the connections of the CFS framing members, self-drilling screws with a diameter of 5.00 mm and a length of 12.70 mm were used. Self-tapping screws with a diameter of 4.00 mm and a length of 25.00 mm were used to fasten the stud member to the chord member. The CFS-wall specimens are illustrated in Fig. 3. The bottom chord

Table 1 Material properties of CFS

CFS	Test No.					Mean	SD	COV
	CFS-1	CFS-2	CFS-3	CFS-4	CFS-5			
t (mm)	0.56	0.55	0.56	0.56	0.55	0.56	0.004	0.007
w (mm)	12.61	12.66	12.59	12.54	12.55	12.59	0.048	0.004
f_y (MPa)	570.60	568.32	584.12	579.55	568.53	574.22	7.189	0.013
f_u (MPa)	620.17	622.32	625.45	625.30	618.33	622.31	3.131	0.005
E_{CFS} (GPa)	213.62	213.88	213.98	213.98	213.89	213.87	0.148	0.001
f_y/f_u	1.09	1.10	1.07	1.08	1.09	1.08	0.009	0.009

where t is the thickness of CFS, w is the width of CFS and E is the modulus of elasticity.

Table 2 Material properties of the screws

Screw	Test No.					Mean	SD	COV
	SC-1	SC-2	SC-3	SC-4	SC-5			
d (mm)	4.89	4.91	4.87	4.87	4.86	4.88	0.020	0.410
f_y (MPa.)	863.00	857.00	866.00	861.00	866.67	862.734	3.940	0.457
f_u (MPa.)	885.25	879.25	888.25	883.25	888.92	884.984	3.940	0.445
E_{screw} (GPa)	204.088	204.012	204.087	204.093	204.089	204.074	7.385	0.004

where d is the diameter of the screw

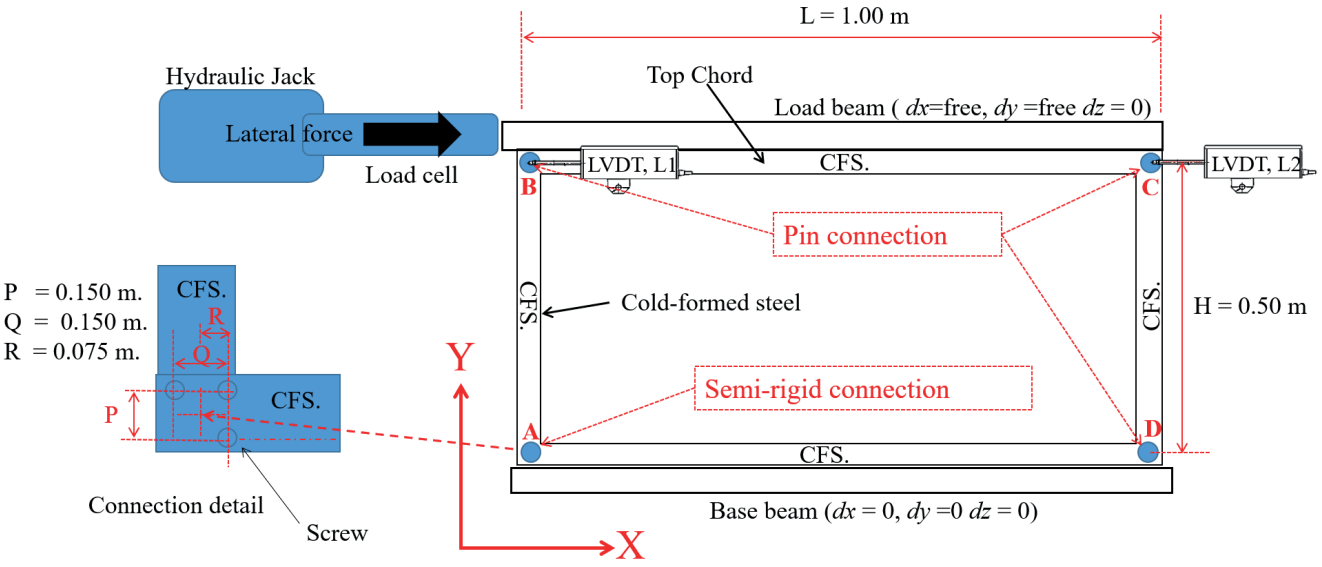

Fig. 1 Schematic diagram of CFS-wall connection test

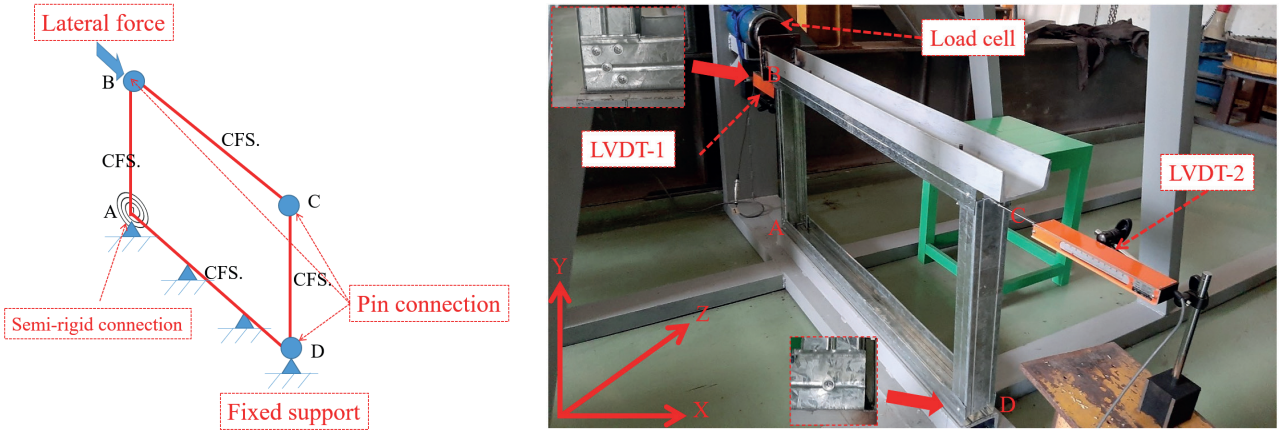

(a) (b)

Fig. 2 Connection test, (a) CFS-well connection test schematic, (b) Connection test set-up

Table 3 CFS-wall test specimens

Specimens	
Name of specimen	Number of repeat tests (*n*)
W-A-n	3
W-B-n	3

of the specimen was attached to the support and the top chord was connected with a load cell by the beam transfer. 3-LVDTs were installed in the vertical stud for measuring the lateral movement. The details of the test setup are shown in Fig. 4.

During testing, the lateral concentrated load was applied incrementally by a hydraulic jack until the observed wall panel buckled and the system lost its stability.

3 Finite element analyses

Finite element analysis (FEA) is a numerical analysis tool that simulates the failure behavior of structures. It has the advantage of saving time and cost in laboratory testing. In this study, the CFS-wall connection and CFS-wall lateral test results were compared with FEA by using the finite element software package Ansys 2020 (Student version) [19].

The geometrical model of FEA was modeled based on the test specimen, including the dimensions of the C-section and the location and diameter of the screw holes. SHELL281 (8-node shell element) with multi-linear isotropic hardening material model being used to model the channel sections. SOLID186 (3-D 20-node solid element) with the linear elastic material model was used to model

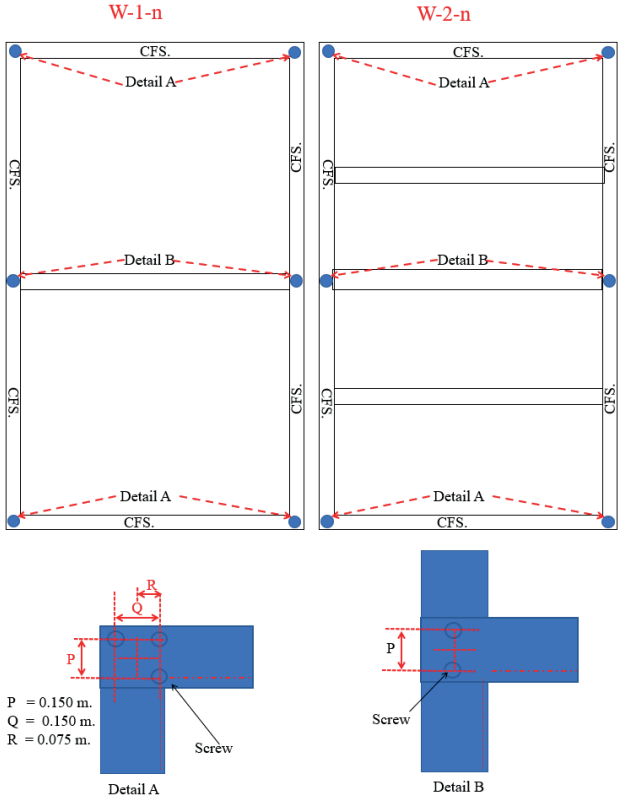

Fig. 3 W-1-UG-n and W-1-G-n specimens

the screws. The contact surfaces between cold-formed steel screwed to cold-formed steel were modeled using CONTA173 and TARGE170 (contact and target). The mesh on the contacting surfaces was assumed to be frictionless for numerical stability [20] and fast matrix operation. Geometrical defects were considered in the analytical approach, which used model Eigen shapes to correct for imperfections [21]. The boundary conditions of the geometry are shown in Fig. 5.

In the problem-solving process, the Newton-Raphson iteration procedure, Line search and time stepping options were used for large deformations analysis [19]. Also, the penalty algorithm was activated to solve the constrained optimization of the contact element [19]. The analysis results were used to verify the experimental results and analytical model.

4 Moment-rotation behaviors of connections

The moment rotation behavior of the interval of the wall connection was analyzed using mathematical models which were based on the test results. In this study, the mathematical model of the moment-rotation relationship referenced the Richard and Abbott model [22] as shown in Fig. 6. The model was represented by the following expression as Eq. (1).

$$M = k_e \phi \Big/ \left(1 + \left(\phi / \phi_e\right)^s\right)^{1/s}, \tag{1}$$

where k_e is the elastic stiffness of the connection, ϕ_e is the rotation stiffness of the connection, and s is the shape parameter (s = 1, 2, 3, …, ∞).

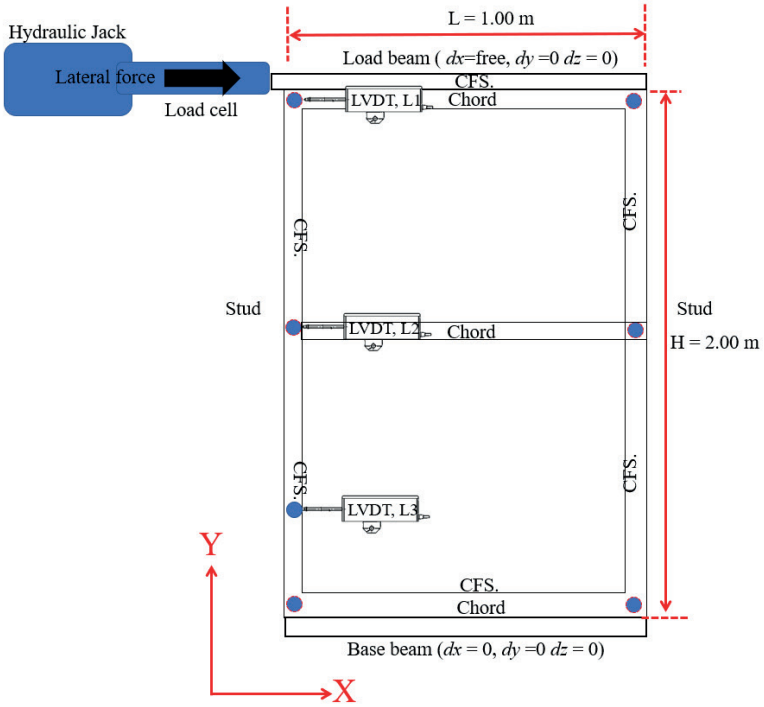

Fig. 4 CFS-wall test set-up

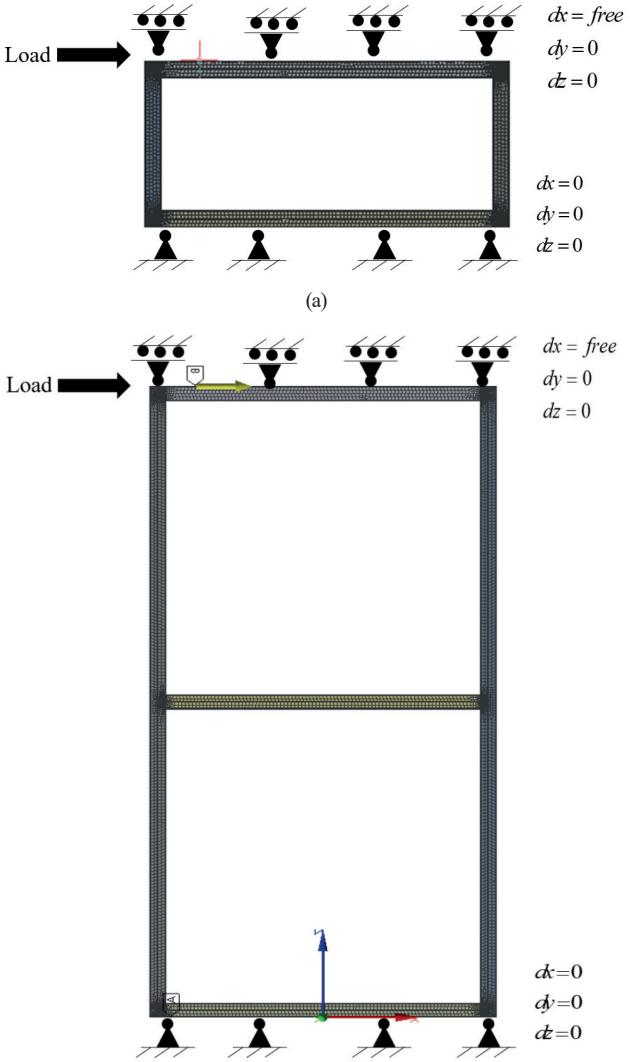

Fig. 5 Boundary conditions of the FE model (a) Boundary conditions of the connection, (b) Boundary conditions of the wall panel

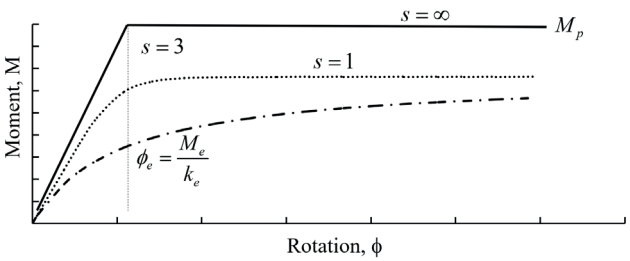

Fig. 6 Richard and Abbott model [22]

The connection of the CFS-wall was simulated as the spring model shown in Fig. 7. The elastic rotational stiffness of the wall panel connection was calculated based on the relationship of the moment-rotation at the centroid of the screw group, which can be written as Eq. (2).

$$k_e = \frac{M_e}{\phi_e} = \frac{\sum_{i=1}^{n} F_i r_i}{\phi_e}, \tag{2}$$

where F_i is the force in the screw, r_i is the distance from the center of rotation to the screw and n is the number of screws in the connection.

The nominal bearing capacity of the screw connection proposed in AISI-S100 [23] can be used to estimate the force in the screw. Where, the nominal bearing capacity was taken as the smaller of Eqs. (3)–(5).

$$F_i = P_{ns} = 4.2\sqrt{t_2^3 d}\, f_{u,2}, \tag{3}$$

$$F_i = P_{ns} = 2.7 t_1 d f_{u,1}, \tag{4}$$

$$F_i = P_{ns} = 2.7 t_2 d f_{u,2}, \tag{5}$$

where P_{ns} is the nominal bearing capacity of the screw connection, t_1 and $f_{u,1}$ are the thickness and nominal yield stress of the member in contact with the screw head, t_2 and $f_{u,2}$ are the thickness and nominal yield stress of the member not in contact with the screw head and d is screw diameter.

The elastic rotation was determined by Eq. (6) which considered the interaction between the screw and the hole.

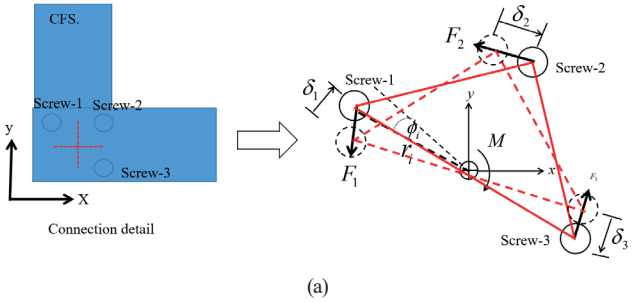

(a)

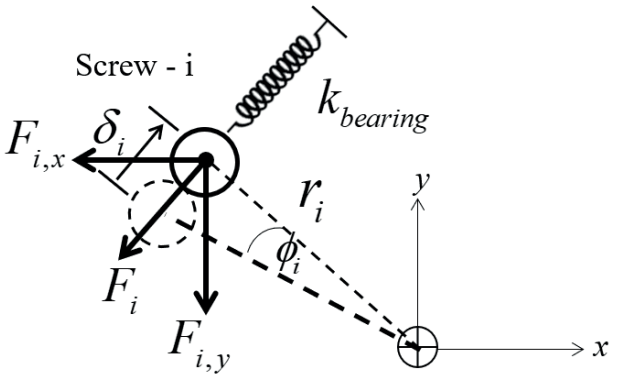

(b)

Fig. 7 Connection stiffness (a) Force and deformation at each bolt-hole, (b) Bearing stiffness and rotation

$$\phi_e = \frac{\sum_{i=1}^{n}\delta_i}{\sum_{i=1}^{n} r_i} = \frac{\sum_{i=1}^{n} F_i}{\sum_{i=1}^{n} r_i k_{bearing,i}}, \tag{6}$$

where ϕ_e is the elastic rotation, δ_i is the deformation of the screw-plate interaction and $k_{bearing}$ is the bearing stiffness between CFS and screw.

The bearing stiffness was calculated by using the schematic diagram of bearing stiffness in Fig. 8 that included screw bearing stiffness ($k_{bea.srew}$) and screw hole bearing stiffness ($k_{bea.hole}$) which can be written as Eq. (7).

$$\frac{1}{k_{bearing}} = \frac{1}{k_{bea,screw}} + \frac{1}{k_{bea,hole}} \tag{7}$$

The screw bearing stiffness ($k_{bea.srew}$) and screw hole bearing stiffness ($k_{bea.hole}$) are presented in Eqs. (8)–(13).

$$\sigma = \frac{f_y}{td}, \tag{8}$$

$$\varepsilon = \frac{\delta}{d}, \tag{9}$$

$$\sigma = E\varepsilon, \tag{10}$$

$$k = \frac{F}{\delta} = tE, \tag{11}$$

$$k_{bea,screw} = tE_{screw}, \tag{12}$$

$$k_{bea,hole} = tE_{CFS}, \tag{13}$$

where σ is the compression stress in the screw and hole, ε is the compression strain in the screw and hole, δ is the deformation, E_{screw} and E_{CFS} are a modulus of elasticity of the screw and CFS.

Finally, the elastic rotational stiffness of the bolt group is presented in Eq. (14).

$$k_{e-i} = \frac{M_{e-i}}{\phi_{e-i}} = \frac{\sum_{i=1}^{n} F_i r_i}{\frac{\sum_{i=1}^{n} F_i}{\sum_{i=1}^{n} r_i k_{bearing,i}}} = \sum_{i=1}^{n} F_i r_i \left(\frac{\sum_{i=1}^{n} r_i k_{bearing,i}}{\sum_{i=1}^{n} F_i} \right) = \sum_{i=1}^{n} r_i^2 k_{bearing,i}, \tag{14}$$

where i is the order of the screw in the connection.

5 CFS-wall connection test and analysis results

The CFS-wall connection test results are shown in Fig. 9 and Table 4. The connection failure was indicated by the specimen entering plastic deformation as the lateral displacement increased and the applied load began to drop.

The test and FEA results presented two failure modes:

1. Bearing failure mode: It was a failure in the borehole region caused by a force that was more than the material allowable stress.
2. Distortional buckling mode: This failure mode was generated by bending forces deforming the cold-formed steel cross-section. As a result, cross-section stability was reduced, and flexural strength was lost.

In Fig. 10, the analytical solution of the moment-rotation was compared to that proposed by experimental tests and FEA. The results show that the analytical model has a good correlation with experimental and FEA data but is lower than these results while undergoing plastic deformation. However, the FEA stiffness was slightly smaller than the test results causing out-of-plane buckling in front of the hole as shown in Fig. 11.

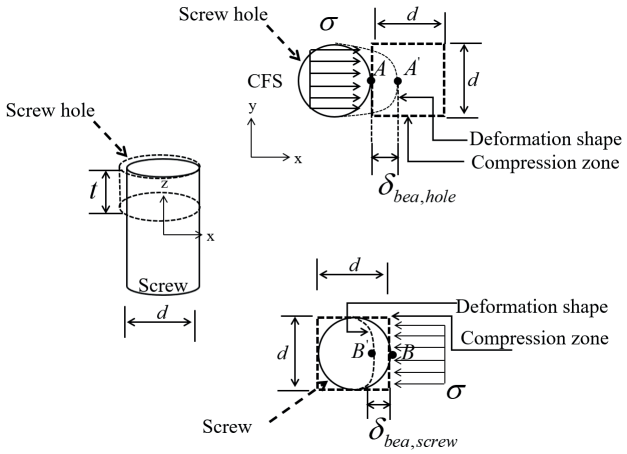

Fig. 8 The bearing stiffness schematic diagram

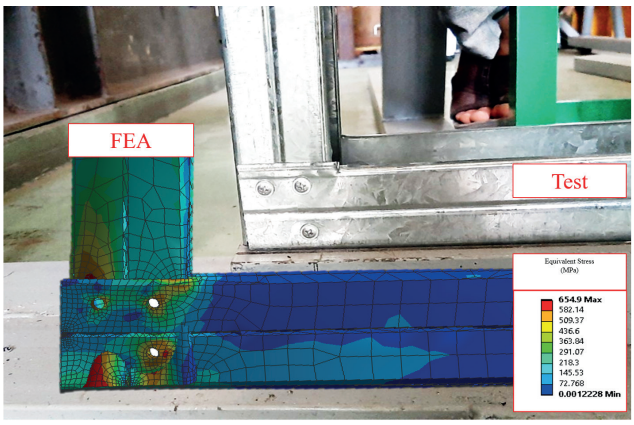

Fig. 9 Connection failure of wall panel connection

Table 4 Connection test results

Sample	Moment capacity (N-m.)			Failure Mode
	Results	Results/Analytical	Results/FEA	
CT-1	992.49	1.12	0.88	Bearing + distortional buckling
CT-2	897.73	1.01	0.80	Bearing + distortional buckling
CT-3	994.76	1.12	0.88	Bearing + distortional buckling
CT-4	950.26	1.07	0.84	Bearing + distortional buckling
CT-5	1063.39	1.20	0.94	Bearing + distortional buckling
CT-Test average	979.73	1.10	0.87	Bearing + distortional buckling
CT-FEA	1126.48	1.27	1.00	Bearing + distortional buckling
CT-Analytical	888.17	1.00	0.79	(Elastic)

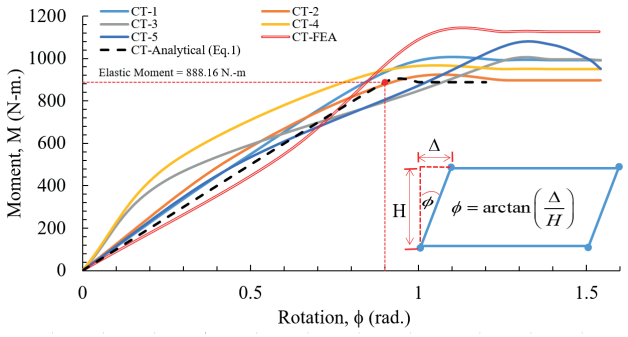

Fig. 10 Moment-rotation curve of wall panel connection test

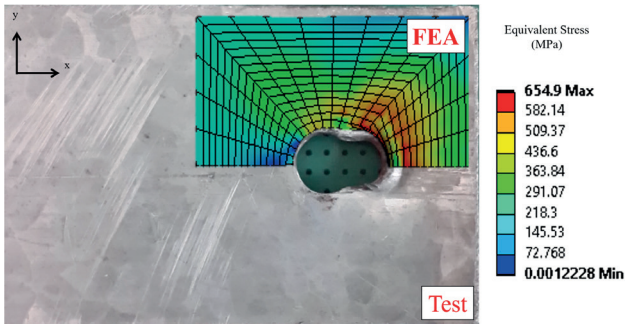

Fig. 11 Out-of-plane buckling in front of the hole

6 Analysis of CFS-wall lateral deformation

As shown in Fig. 12, the external lateral force was applied at the top of the corner stud member (Point 5). Under the action of the lateral force, elastic lateral deflection (Δ_x) of the CFS-wall occurred due to the rotation of the structural members relative to each other at the connections, and the bending of the stud members. All the columns in the wall system carry the lateral load at their top. These can be simplified to a single-column spring model as shown in Fig. 13. The column was simplified by the guide cantilever beam with a rotation spring element at the connection. Based on the elastic moment - rotation of the connection, the limited bending moment can be obtained from the test results (Fig. 10). Thus, the rotation angle of the beam-to-column connection was calculated by Eqs. (15)–(16)).

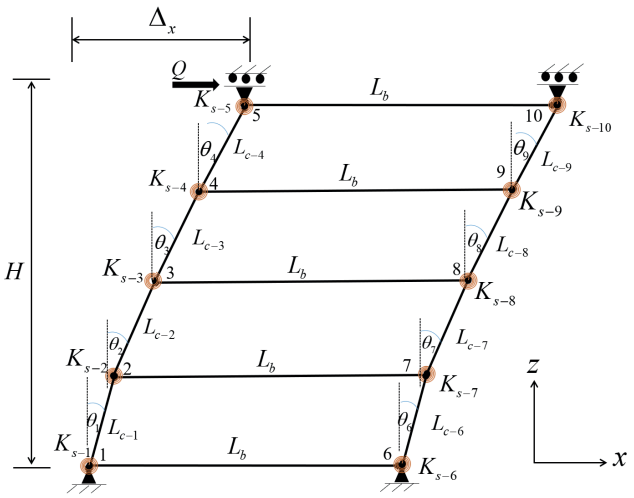

Fig. 12 Wall model

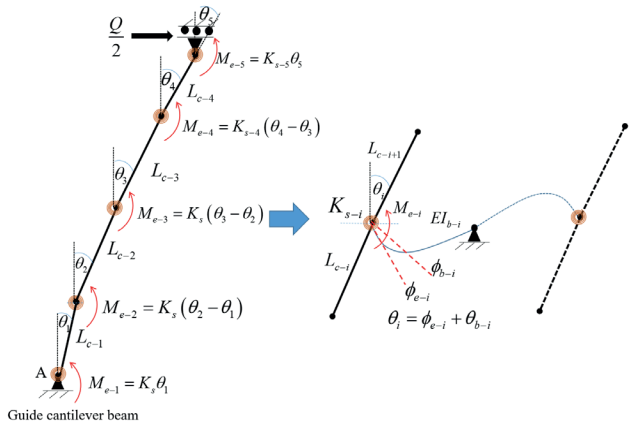

Fig. 13 Simplified to a single-column spring model

$$\theta_j = \frac{M_{e-j}}{K_{s-j}}, \tag{15}$$

$$\theta_j = \phi_{e-j} + \phi_{b-j}, \tag{16}$$

where ϕ_e is the rotation stiffness of connection (Eq. (16)), where j is the order of the connection and θ_b is the rotation angle of the beam (Eqs. (17)–(18).

$$\phi_{e-j} = \frac{1}{k_{e-j}}, \tag{17}$$

$$\phi_{b-j} = \frac{1}{\left(6EI_{b-j}/L_{b-j}\right)} = \frac{1}{k_{b-j}}, \tag{18}$$

where EI_b is a flexural rigidity of the beam and L_b is the length of the beam.

The rotational stiffness (K_{s-j}) of springs in the single-column model considering the deformation of portal beams was calculated by Eq. (19).

$$\frac{1}{K_{s-j}} = \frac{1}{k_{e-j}} + \frac{1}{k_{b-j}} \tag{19}$$

Thus

$$\frac{1}{K_{s-j}} = \frac{1}{k_{e-j}} + \frac{1}{6EI_{b-j}/L_{b-j}^2} \tag{20}$$

The lateral deformation of a single-column spring model due to a rotation spring element at the connection is written as Eq. (21). Under the assumption of small deflection conditions, the Eq. (21) can be rewritten as Eq. (22).

$$\begin{aligned} &L_{c-1}\sin\theta_1 + L_{c-2}\sin\theta_2 + L_{c-3}\sin\theta_3 \\ &+L_{c-4}\sin\theta_4 = \sum_{j=1}^{m} L_{c-j}\sin\theta_j = \Delta_{x-Spring} \end{aligned} \tag{21}$$

$$\begin{aligned} &L_{c-1}\theta_1 + L_{c-2}\theta_2 + L_{c-3}\theta_3 \\ &+L_{c-4}\theta_4 = \sum_{n=1}^{m} L_{c-i}\theta_i = \Delta_{x-Spring} \end{aligned} \tag{22}$$

The elastic lateral deformation at the end of the single-column spring model ($\Delta X_{\max}$) can be derived from the sum of the lateral deformation due to a rotation spring element at the connection ($\Delta_{x-Spring}$) and the elastic deformation of the guide cantilever beam equation ($\Delta_{x-Elastic}$) as shown in Eq. (23).

$$\Delta X_{\max} = \Delta_{x-Elastic} + \Delta_{x-Spring}, \tag{23}$$

where

$$\Delta_{x-Elastic} = \frac{Q}{2}\left(\frac{H^3}{12EI}\right), \tag{24}$$

where Q is an elastic lateral load, H is the height of the wall and EI is a flexural rigidity [24]. Finally, the equation for the elastic lateral deformation of the single-column spring model was written as shown in Eq. (25):

$$\Delta X_{\max} = \frac{QH^3}{12EI} - \sum_{j=1}^{m} L_{c-j}\theta_j = \frac{QH^3}{12EI} - \sum_{j=1}^{m} L_{c-j}\left(\frac{M_{e-j}}{K_{s-j}}\right). \tag{25}$$

7 CFS-wall test and analysis results

The proposed elastic lateral deformation was compared with FEA and the experimental test. The lateral deformation by the analytical model was compared with the LVDT, L1 result (Top chord).

W-A-n failed due to the combined distortional buckling at the column, and the connection failure, as shown in Fig. 14. The comparison of the load-deformation curves is shown in Fig. 15.

W-B-n failed due to the combined distortional buckling at the column and the connection failure, as shown in Fig. 16. The comparison of the load-deformation curves is shown in Fig. 17. The results of the tests are summarized in Table 5. The failure mode of CFS-wall specimens was combined with the distortional buckling mode and connection failure mode. The distortional buckling was a mode described by the rotation of the flange at the flange-web junction in CFS-members with edge-stiffened elements.

In the test results, the distortional buckling was characterized by the closing up of the two flanges. The connection failure mode at the borehole region was caused by a force that was more than the plate material yield strength which occurred in the bolt hole failure. The failure controlled the behavior of a CFS-wall specimen was the connection failure mode. In the lateral load - lateral displacement curves, the lateral load initially increases and passed the maximum when the connection failed. Beyond the maximum point, the failure of CFS-wall specimens was controlled by combining the distortional buckling mode and connection failure mode that caused the large lateral deformation.

The proposed elastic lateral stiffness was compared with FEA and experimental tests. The comparison of the results of the load-deformation curve showed that the proposed equation was in good correlation with the experiment results and FEA.

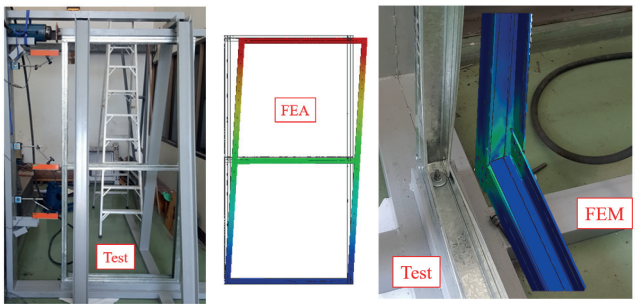

(a) (b)

Fig. 14 Failure mode of W-A-n (a) lateral deformation on a specimen and FEA, (b) failure mode of connection

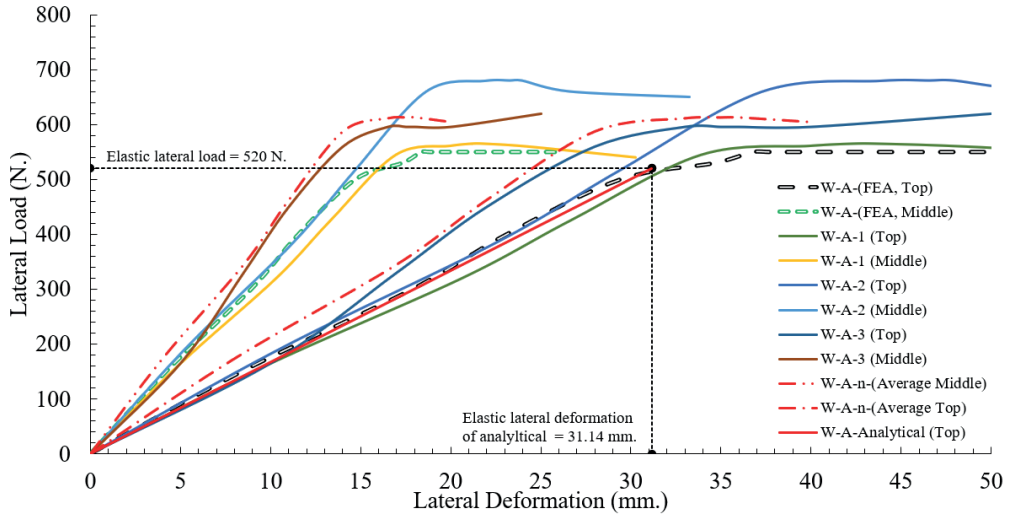

Fig. 15 comparison of the load-deformation of W-A-n

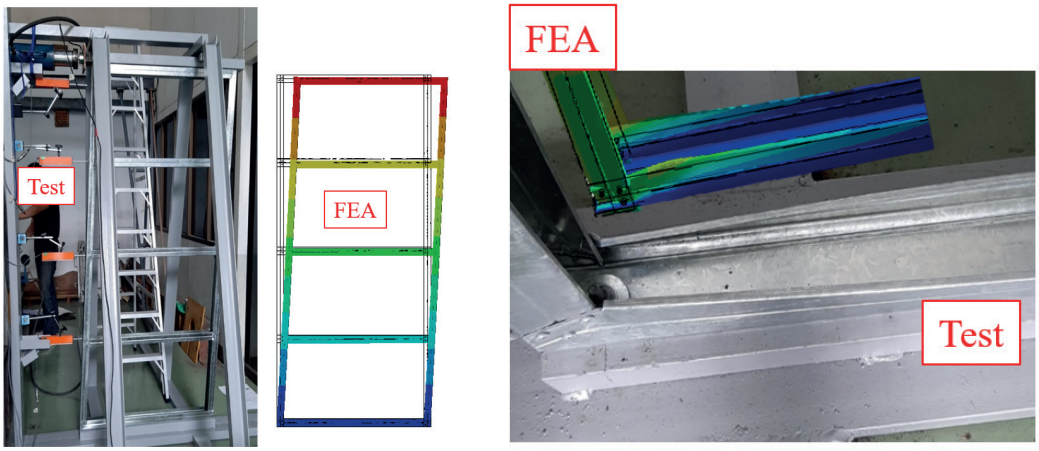

(a) (b)

Fig. 16 Failure mode of W-B-n (a) lateral deformation on specimen and FEA, (b) failure mode of joint

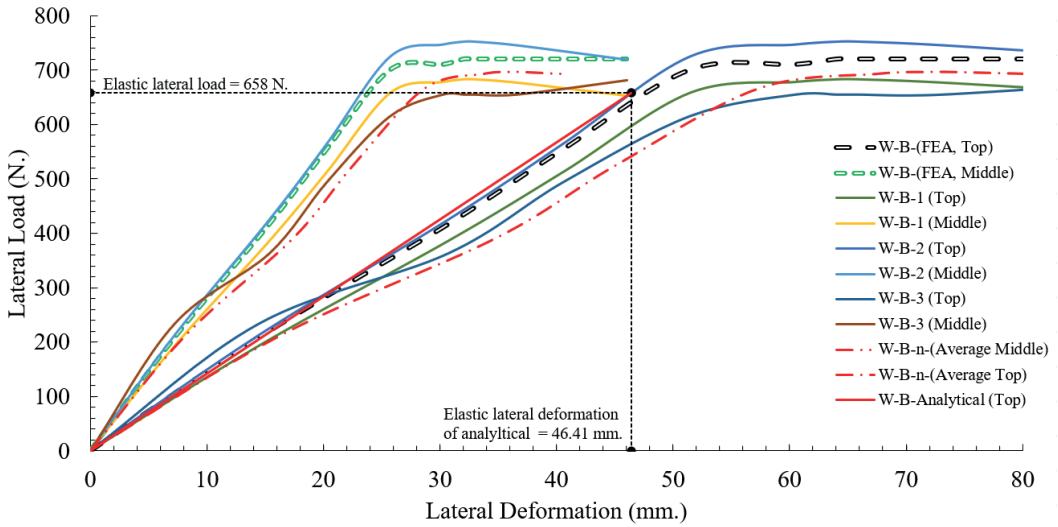

Fig. 17 comparison of the load-deformation W-B-n

Table 5 lateral wall test results

Lateral load capacity (N.)			Test/FEA	Failure mode
Test	FEA	Analytical		
565.00			1.09	distortional buckling + connection failure
680.00	550.00	520.00	1.31	distortional buckling + connection failure
620.00			1.19	distortional buckling + connection failure
683.65			1.04	distortional buckling + connection failure
752.02	720.00	658.00	1.14	distortional buckling + connection failure
682.00			1.04	distortional buckling + connection failure

8 Conclusions

An elastic lateral stiffness equation for the CFS-wall was proposed in this study. The proposed equation was evaluated against the predicted values using experimental results and a finite element model. In the experimental test procedure, the tests were divided into 2 sections, first as a wall connection test and then a full-scale wall panel structure test. The failure mode CFS-wall connection test presented two failure modes as the bearing failure mode and distortional buckling mode. CFS-wall the combined failure mode between bearing failure mode and distortional buckling mode controlled the failure behavior. All test results were compared by FEA. The comparison results show a good correlation between the tests and FEA.

The analytical methods for a CFS-wall connection and CFS-wall lateral deformation were proposed. In the analytical wall connection model, the analytical model has developed the elastic rotational stiffness of the bolt-group using the spring model. The accuracy of the results from the analytical wall connection model was verified by experimental test and the FEA, with a high correlation between the three.

In the analytical CFS-wall model, the single-column spring model was used to analyze the CFS-wall lateral deformation. The single-column spring model was formed by combinations of a guide cantilever beam and springs connection, and the spring constants were determined by using the stiffness of the connection and the bending stiffness of the chord. The experiments tests and FEA were conducted to verify the analytical model. The comparison of results showed good agreement between the analytical prediction, FEA and experimental data in the case of the primary type of cold-formed wall structure.

The proposed procedure was an efficient method for elastic lateral deformation analysis of CFS-wall which can be used for all wall panel structure configurations.

Acknowledgment

The authors wish to acknowledge the National Research Council of Thailand (NRCT) for providing funding support and Mr. Roy I. Morien, of the Naresuan University Graduate School, for his assistance in editing the English expression and grammar in this paper.

References

[1] Konkong, N., Aramraks, T., Phuvoravan, K. "Buckling length analysis for compression chord in cold-formed steel cantilever truss", International Journal of Steel Structures, 17, pp. 775–787, 2017.
https://doi.org/10.1007/s13296-017-6031-7

[2] Bešević, M., Prokić, A., Landović, A., Kasaš, K. "The Analysis of Bearing Capacity of Axially Compressed Cold Formed Steel Members", Periodica Polytechnica Civil Engineering, 61(1), pp. 88–97, 2017.
https://doi.org/10.3311/PPci.8836

[3] Mahi, I., Djelil, M., Djafour, N., Djafour, M. "Calculation of Critical Load for Pure Distortional Buckling of Lipped Channel Columns", Periodica Polytechnica Civil Engineering, 63(4), pp. 1016–1029, 2019.
https://doi.org/10.3311/PPci.13244

[4] Nithyadharan, M., Kalyanaraman, V. "Behaviour of cold-formed steel shear wall panels under monotonic and reversed cyclic loading", Thin-Walled Structures, 60, pp. 12–23, 2012.
https://doi.org/10.1016/j.tws.2012.05.017

[5] Dewangan, A., Bhatt, G., Sonkar, C. "Axial Strength Estimation of Cold Formed Steel Wall Panels Through Numerical Modeling", In: Emerging Trends in Civil Engineering, Springer, 2020, pp. 91–100. ISBN: 978-981-15-1403-6

[6] Wang, C., Yang, Z., Zhang, Z., Qi, R. "Experimental study on shear behavior of cold-formed steel shear walls with bracket", Structures, 32, pp. 448–460, 2021.
https://doi.org/10.1016/j.istruc.2021.03.064

[7] Derveni, F., Gerasimidis, S., Peterman, K. "Behavior of cold-formed steel shear walls sheathed with high-capacity sheathing", Engineering Structures, 225, 111280, 2020.
https://doi.org/10.1016/j.engstruct.2020.111280

[8] ANSI "AISI-S400-15 North American standard for seismic design of cold-formed steel structural systems", American Iron and Steel Institute, Washington, DC, USA, 2015.

[9] Liu, P., Peterman, K. D., Schafer, B. W. "Impact of construction details on OSB-sheathed cold-formed steel framed shear walls", Journal of Constructional Steel Research, 101, pp. 114–123, 2014. https://doi.org/10.1016/j.jcsr.2014.05.003

[10] Niari, S. E., Rafezy, B., Abedi, K. "Seismic behavior of steel sheathed cold-formed steel shear wall: Experimental investigation and numerical modeling", Thin-Walled Structures, 96, pp. 337–347, 2015. https://doi.org/10.1016/j.tws.2015.08.024

[11] Mohebbi, S., Mirghaderi, R., Farahbod, F., Sabbagh, A. B. "Experimental work on single and double-sided steel sheathed cold-formed steel shear walls for seismic actions", Thin-walled Struct, 91, p. 50–62, 2015. https://doi.org/10.1016/j.tws.2015.02.007

[12] Gao, W. C., Xiao, Y. "Seismic behavior of cold-formed steel frame shear walls sheathed with ply-bamboo panels", Journal of Constructional Steel Research, 132, pp. 217–229, 2017. https://doi.org/10.1016/j.jcsr.2017.01.020

[13] Javaheri-Tafti, M. R., Ronagh, H. R., Behnamfar, F., Memarzadeh, P. "An experimental investigation on the seismic behavior of cold-formed steel walls sheathed by thin steel plates", 80, pp. 66–79, 2014. https://doi.org/doi:10.1016/j.tws.2014.02.018

[14] Zeynalian, M., Ronagh, H. R. "Seismic performance of cold formed steel walls sheathed by fiber-cement board panels", Journal of Constructional Steel Research, 107, pp. 1–11, 2015. https://doi.org/10.1016/j.jcsr.2015.01.003

[15] AISI "AISI S213 North American standard for cold-formed steel framing-Lateral design", American Iron and Steel Institute, Washington, DC, USA, 2007.

[16] ECCS "Recommended testing procedure for assessing the behavior of structural elements under cyclic loads", European Convention for Constructional Steelwork, Brussels, Belgium, 1986.

[17] ASTM "ASTM A370-20 Standard Test Methods and Definitions for Mechanical Testing of Steel Products", ASTM International, West Conshohocken, PA, USA, 2020. https://doi.org/10.1520/A0370-20

[28] ASTM "ASTM C1513-18 Standard Specification for Steel Tapping Screws for Cold-Formed Steel Framing Connections", ASTM International, West Conshohocken, PA, USA, 2018. https://doi.org/10.1520/C1513-18

[19] ANSYS Inc "Ansys 2021", [software] 2021. Available at: https://www.ansys.com/

[20] Jakab, G., Dunai, L. "Laboratory and virtual experiments on C-section compression members with semi-rigid connections", Periodica Polytechnica Civil Engineering, 51(1), pp. 31–43, 2010. https://doi.org/10.3311/pp.ci.2010-1.04

[21] Woodward, J. "Eigenvalue Buckling and Post-buckling Analysis in ANSYS Mechanical", PADT, Inc., 2018. [online] Available at: https://www.padtinc.com/blog/eigenvalue-buckling-and-post-buckling-analysis-in-ansys-mechanical

[22] Richard, R. M., Abbott, B. J. "Versatile elastic plastic stress-strain formula", Journal of the Engineering Mechanics Division, 101(4), pp. 511–515, 1975. https://doi.org/10.1061/JMCEA3.0002047

[23] ANSI "AISI S100 North American Specification for the Design of Cold-Formed Steel Structural Members", American Iron and Steel Institute, Washington, DC, USA, 2015.

[24] Bhave, S. U., Sonawane, P. "Analysis of Pump Piping Based on Piping Configurations", International Journal for Innovative Research in Science & Technology, 2(9), pp. 28–34, 2016.